Arch. Mech., **62**, 1, pp. 21–48, Warszawa 2010

Viscoelasticity and fractal structure in a model of human lungs

C. M. IONESCU[1)], W. KOSIŃSKI[2)], R. DE KEYSER[1)]

[1)] *Department of Electrical Energy, Systems and Automation*
Ghent University
Technologiepark 913, Gent 9052, Belgium
e-mails: ClaraMihaela.Ionescu@UGent.be, Robain.DeKeyser@UGent.be

[2)] *Department of Computer Science*
Polish-Japanese Institute of Information Technology
Koszykowa 86, 02-008 Warszawa, Poland
and
Institute of Mechanics and Applied Computer Science
Kazimierz Wielki University in Bydgoszcz
Chodkiewicza 30, 85-064 Bydgoszcz, Poland
e-mail: wkos@pjwstk.edu.pl

THIS PAPER PROVIDES a model of the human respiratory system by taking into account the fractal structure of the airways and the viscoelastic properties of the tissue. The self-similarity of airway distribution is admitted up to the 24th generation. Due to periodic breathing which results in sinusoidal excitation of the respiratory system, an electrical equivalent model is developed. The periodic current in this electrical network, that preserves the geometry of the human respiratory tree, is equivalent to the oscillatory air-flow. The model is expressed by Navier–Stokes equations under cylindrical symmetry, linked with an equation responsible for the motion of viscoelastic tissue of airway walls. By use of both electro-mechanical analogies, the total impedance of the respiratory system is determined and compared to the measured data in the clinical range of 4–48 Hz, as well as in the low-frequency range of 0.1–5 Hz. We propose also a lumped model of fractional orders, which is able to capture frequency-dependent variations in both clinical as well as in the low-frequency ranges. The models proposed in this paper can be further used to determine the effects of disease on the lung morphology.

Key words: respiratory system, airways, Navier–Stokes flow, viscoelastic properties, morphology, electrical transmission lines, input impedance.

Notations

δ Womersley parameter $= R\sqrt{\omega\rho/\mu}$,
$\acute{\epsilon}_{10}$, $\acute{\acute{\epsilon}}_{10}$ phase angle of the complex number from Bessel functions of rank 1 and order 0, respectively 1,
ϕ, φ phase angle,
γ complex propagation coefficient,
κ cartilage fraction,

λ wavelength,
ψ damping factor,
μ dynamic viscosity,
ν_P coefficient of Poisson (= 0.45),
θ contour coordinate,
$\rho, \rho_{\text{wall}}, \rho_s, \rho_c$ density of air at BTPS, respectively of the airway wall of the soft tissue and of the cartilage,
ω angular frequency,
ζ radial deformation,
c_x capacity per distance unit,
$\tilde{c}, \acute{c}_0, c_0$ the complex velocity of wave propagation, the effective/corrected Moens–Korteweg velocity an the nominal Moens–Korteweg velocity,
f frequency in Hz,
g_x conductance per distance unit,
h wall thickness,
i complex unit $= \sqrt{-1}$,
l_x inductance per distance unit,
m airway depth,
p pressure,
q flow,
r radial direction, radial coordinate,
r_x resistance per distance unit,
t time,
u velocity in radial direction,
v velocity in contour direction,
w velocity in axial direction,
z axial direction, longitudinal coordinate,
y ratio of radial position to radius $= r/R$,
C_e compliance,
E^*, E_s, E_c complex elasticity modulus, respectively for soft and cartilage tissue,
G_e conductance,
J Bessel function,
ℓ airway length,
L_e inertance,
M modulus for pressure gradient,
$\acute{M}_{10}, \acute{M}_{10}$ modulus of the complex number from Bessel functions of rank 1 and order 0, respectively 1,
P pressure,
q flow,
R_e resistance,
R airway inner radius,
Z_l, Z_t longitudinal, respectively transversal impedance.

1. Introduction

Lung geometry and morphology have been studied in the past from lung casts and nowadays they have been validated using CT scans in 3D form [31, 32]. Already since Weibel in 1963 [39], the fractal geometry present in the lung morphology has been employed in studies on lung aerodynamics. It is significant to

note that the self-similarity is related to the optimality of ventilation and that asymmetry exists in the healthy lung as well, whereas a diseased lung contains significant heterogeneities and the optimality conditions are not fulfilled anymore [12]. The ultimate goal of this study is to relate human lung morphology to the properties of dynamic systems posing a fractal geometrical structure.

One of the most comprehensive and earliest overviews on the mechanical properties of lungs is given by MEAD in [22], describing the initial attempts to quantify static and dynamic resistive, inertial and compliant properties of lungs. His review covers both the inspiratory and expiratory phase, at laminar and turbulent flow conditions, in terms of a single variable: the air volume. Another important study has been reported in [26] for tube-entrance flow and pressure drop during inspiration under spontaneous ventilation conditions. In the study performed by PEDLEY in [29] to assess the flow and pressure drop in branching airways, an important finding is that during spontaneous ventilation (unforced breathing in relaxed conditions, also referred to as tidal breathing), the air flow remains laminar (typical Reynolds number below 2000) [12, 26, 29].

Based on the technological and the computational progress, SAURET *et al.* performed a study based on CT scans of the 3D-topology and morphology of a human (cast) lung [31, 32]. Mean gravity and branching angles up to level 9 generations for the right and left lobe (asymmetric morphology due to heart location) were reported. The present model differs from the previously reported models in that it introduces the assumption of flexible airways in a simple form, taking into account the wall tissue structure (in terms of cartilage and soft tissue percent and densities) and derives the mechanical parameters to directly illustrate changes in airway morphology with disease. The resulting model is therefore relatively simple and efficient to capture the intrinsic viscoelastic properties in an electrical equivalent. There are several assumptions which are generally accepted from previous studies and used here as simplifying assumptions [9, 22]. The first assumption is that the pressure at the boundaries of all parts is the same at all points of the respective boundaries. The next: three of the boundaries contain gas only on one side: airway opening, alveolar surface and body surface. Uniform pressure is valid if the gas is in continuity condition and no flow. These conditions are fulfilled for the body surface, during panting at the airway opening and the alveoli. The only part which is not in agreement with this hypothesis is the pleural surface, which has tissue on both sides and its pressure distribution cannot be predicted. The work presented in this paper is based on laminar flow conditions [12, 26, 29], which are indeed valid during tidal breathing.

The contribution of this work consists in deriving a model which combines tidal breathing conditions and lung morphology. Although the theoretical basis has been previously employed in modelling of the circulatory system under similar assumptions [27], the model proposed here allows to make variations in the

lung's morphology as expected in specific pathologies. Making use of the fractal geometry of the respiratory tree and theoretical development for modelling the circulatory tree, a mathematical model has been developed to characterize the dynamics of respiratory pressure and flow [17]. The electrical analogy for viscoelastic airways proposed here, provides insight into changes in resistance, inertance, compliance and conductance parameters in healthy and diseased airways, where rheological properties play an important role. The procedure used here allows to determine the correspondence between the electrical and mechanical parameters such as resistance, inertance, compliance and conductance of the respiratory input impedance.

The original contribution of this work is the introduction of viscous loses into the mechano-electrical equivalent model representation. It is important to quantify this aspect since the heterogeneity of the lung parenchyma is increasing with pathology, and hence viscous loses become important. The previous model consisting solely of elastic components will not be able to capture the changes in the respiratory impedance with disease [17]. The work of breathing, i.e. the energy necessary to be posed by the system to perform the respiratory function is increasing, if there is a more viscous, stiff, scarred lung tissue (e.g. fibrosis, emphysema).

The paper is further divided into four sections: the model for the pressure and flow in the airways considered with viscoelastic wall properties, with specific morphologic parameters, the electrical equivalent representation, the results of these models and discussion. A conclusion section summarizes the outcome of this work and gives a short summary of its prospective use.

2. Materials and methods

2.1. Mathematical modelling of pressure-flow dynamics

For the case when sinusoidal excitation is applied to the respiratory system, one may analyze the oscillatory flow conditions [15, 28, 9]. To find an electrical equivalent of the respiratory duct, one needs the expressions relating pressure and flow to properties of the viscoelastic tubes, which can be done straightforward via the Womersley theory [2, 27]. Analogue to the Womersley theory from circulatory system analysis, which considers the pulsatile flow in a circular pipeline, for varying pressure-gradient, the periodic breathing (usually, for normal breathing conditions, around 4 s) can be defined as a function of modulus and phase, i.e. as a periodical function. Since the input to the respiratory system is the pressure gradient, first we have to give the pressure gradient at $z = 0$ in terms of a periodical function

$$-\frac{\partial p}{\partial z} = \mathrm{Re}[Me^{i(\omega t-\phi)}] = M\cos(\omega t - \phi), \tag{2.1}$$

where z is the axial direction, longitudinal coordinate, $i = \sqrt{-1}$, $\omega = 2\pi f$ is the angular frequency (rad/s), with f the frequency (Hz), M the modulus and ϕ is the phase angle of the pressure gradient. Given its periodicity, it follows that the pressure and other velocity components will also be periodic, with the same angular frequency ω, the velocity in radial direction $u(r, z, t)$, the velocity in the axial direction $w(r, z, t)$, the pressure $p(r, z, t)$, the dimensionless parameter $y = r/R$, $0 \leq y \leq 1$ denoting the ratio of the radial position with respect to the axis of the tube are employed, along with all variables from Table 1 that represents the tube parameters of each generation.

Table 1. The tube parameters for the sub-glottal airways generations, whereas 1 denotes the trachea and 24 the alveoli, as from [12, 13, 20, 23, 39, 40].

Generation m	Length ℓ (cm)	Radius R (cm)	Wall thickness h (cm)	Cartilage fraction κ
1	10.0	0.80	0.3724	0.67
2	5.0	0.6	0.1735	0.5000
3	2.2	0.55	0.1348	0.5000
4	1.1	0.40	0.0528	0.3300
5	1.05	0.365	0.0409	0.2500
6	1.13	0.295	0.0182	0.2000
7	1.13	0.295	0.0182	0.0922
8	0.97	0.270	0.0168	0.0848
9	1.08	0.215	0.0137	0.0669
10	0.950	0.175	0.0114	0.0525
11	0.860	0.175	0.0114	0.0525
12	0.990	0.155	0.0103	0.0449
13	0.800	0.145	0.0097	0.0409
14	0.920	0.140	0.0094	0.0389
15	0.820	0.135	0.0091	0.0369
16	0.810	0.125	0.0086	0.0329
17	0.770	0.120	0.0083	0.0308
18	0.640	0.109	0.0077	0.0262
19	0.630	0.100	0.0072	0.0224
20	0.517	0.090	0.0066	0.0000
21	0.480	0.080	0.0060	0.0000
22	0.420	0.070	0.0055	0.0000
23	0.360	0.055	0.0047	0.0000
24	0.310	0.048	0.0043	0.0000

The air in the airways is treated as Newtonian, with constant viscosity $\mu = 1.8{\cdot}10^{-5}$ kg/m-s and density $\rho = 1.075$ kg/m^3. Applying Navier–Stokes equations in cylindrical coordinates [41], under the assumption of axi-symmetrical flow in a cylindrical pipeline, air in the lungs is incompressible, and with vanishing external body forces, we have:

$$\rho\left(\frac{\partial u}{\partial t}+u\frac{\partial u}{\partial r}+w\frac{\partial u}{\partial z}\right)=-\frac{\partial p}{\partial r}+\mu\left[\frac{1}{r}\frac{\partial}{\partial r}\left(r\frac{\partial u}{\partial r}\right)-\frac{u}{r^2}+\frac{1}{r^2}\frac{\partial^2 u}{\partial\theta^2}-\frac{\partial^2 u}{\partial z^2}\right] \tag{2.2}$$

for the radial direction r, and

$$\rho\left(\frac{\partial w}{\partial t}+u\frac{\partial w}{\partial r}+w\frac{\partial w}{\partial z}\right)=-\frac{\partial p}{\partial z}+\mu\left[\frac{1}{r}\frac{\partial}{\partial r}\left(r\frac{\partial w}{\partial r}\right)+\frac{\partial^2 w}{\partial z^2}\right] \tag{2.3}$$

in the axial direction z, and

$$\frac{u}{r}+\frac{\partial u}{\partial r}+\frac{\partial w}{\partial z}=0 \tag{2.4}$$

as the continuity (incompressibility) equation. Dividing by the density ρ, observing that air in airways has very low total pressure drop variations, ≈ 0.1 kPa [26], and using the relation $y = r/R$ to substitute the partial derivative with respect to r by $\partial/\partial y$, and considering the further simplifying assumptions:

(i) the radial velocity component is small, as well as the ratio u/R and the term in the radial direction;

(ii) the terms $\partial^2/\partial z^2$ in the axial direction are negligible.

The following system is reached:

$$\frac{\partial u}{\partial t}=-\frac{1}{\rho R}\frac{\partial p}{\partial y}+\frac{\mu}{\rho}\left[\frac{1}{yR^2}\frac{\partial u}{\partial y}+\frac{1}{R^2}\frac{\partial^2 u}{\partial y^2}-\frac{u}{R^2y^2}\right], \tag{2.5}$$

$$\frac{\partial w}{\partial t}=-\frac{1}{\rho}\frac{\partial p}{\partial z}+\frac{\mu}{\rho}\left[\frac{1}{yR^2}\frac{\partial w}{\partial y}+\frac{1}{R^2}\frac{\partial^2 w}{\partial y^2}\right], \tag{2.6}$$

$$\frac{u}{Ry}+\frac{1}{R}\frac{\partial u}{\partial y}+\frac{\partial w}{\partial z}=0. \tag{2.7}$$

Studies on the respiratory system using similar simplifying conditions can be found in [9, 26, 29]. Given the periodicity of the pressure gradient in (2.1), it follows that also the pressure $p(y, z, t)$ and the other velocity components $u(y, z, t)$, $w(y, z, t)$ are periodic in time and z variable, as in:

$$\begin{aligned} p(y,z,t) &= p_1(y)e^{i\omega(t-z/\tilde{c})},\\ u(y,z,t) &= u_1(y)e^{i\omega(t-z/\tilde{c})},\\ w(y,z,t) &= w_1(y)e^{i\omega(t-z/\tilde{c})}, \end{aligned} \tag{2.8}$$

where $\tilde{c}$ denotes the complex velocity of wave propagation and for the solution, the real parts of the right-handed sides of (2.8) should be taken. Introducing in (2.6) the solution given for p and w in (2.8), one obtains the following differential equation:

$$\frac{d^2w_1(y)}{dy^2}+\frac{dw_1(y)}{ydy}-\frac{i\omega\rho R^2}{\mu}w_1(y)=-\frac{i\omega\rho R^2}{\mu\rho\tilde{c}}p_1(y). \tag{2.9}$$

Its solution is given by

$$w_1(y) = C_1 J_0(\lambda y) + \frac{i\omega R^2}{\mu\tilde{c}(\lambda^2 - k^2)} p_1(y),$$

with C_1 being a complex integration constant, J_0 a Bessel function of the 1st kind and 0 degree, and k an arbitrary constant which is to determine via the continuity equation (2.7) and $\lambda^2 = i^3\delta^2$ with the Womersley parameter δ, defined as the dimensionless parameter $\delta = R\sqrt{\omega\rho/\mu}$ [17, 43]. The further detailed procedure of finding the solutions for p_1 and u_1 is described in [34] where all equations (2.5)–(2.7) are used. It turns out that the constant $k = i\omega R/\tilde{c}$ is a measure of proportionality of the tube radius to the wavelength of a pressure wave ($\tilde{c}/2\pi f$), and resulting in small values. For the tracheal respiratory tube where $R = 0.008$m and for the breathing frequency of 0.2–5 Hz, the wavelength is about 2.5 m. Further simplifications lead to the following forms of solution:

$$u(y,z,t) = \frac{i\omega R}{\mu\tilde{c}}\left\{C_1\frac{2}{\lambda}J_1(\lambda y) + \frac{A}{\rho\tilde{c}}y\right\}e^{i\omega(t-z/\tilde{c})}, \tag{2.10}$$

$$w(y,z,t) = \left\{C_1 J_0(\lambda y) + \frac{A}{\rho\tilde{c}}\right\}e^{i\omega(t-z/\tilde{c})}, \tag{2.11}$$

$$p(1,z,t) = Ae^{i\omega(t-z/\tilde{c})} \qquad \text{or} \qquad -\frac{\partial p}{\partial z} = Me^{i(\omega t-\phi)}, \tag{2.12}$$

with $C_1 = -A/J_0(\lambda)\rho\tilde{c}$, J_1 a Bessel function of rank 1 and the 1st degree, and

$$-\frac{\partial p}{\partial z} = \frac{i\omega}{\tilde{c}}Ae^{i\omega(t-z/\tilde{c})} = Me^{i(\omega t-\phi)}\,.$$

Hence due to (2.1), the compatibility condition is $Ae^{i\omega(t-z/\tilde{c})} = \dfrac{\tilde{c}}{\omega}Me^{i(\omega t-\phi-\pi/2)}$. The coefficients A and M will be determined from the interface and boundary conditions.

2.2. Viscoelasticity of airways wall

The boundary condition linking the wall and pipeline equations is the no-slip condition that assumes the fluid particles adherent to the inner surface of the airway, and hence to the motion of the viscoelastic wall.

The viscoelasticity of the wall is determined by the rheological properties of the tissue. Hence, it depends on the amount of cartilage fraction in the tissue, as the viscous component (collagen), or by the soft tissue fraction in the tissue as the elastic component (elastin) [6]. Taking into account at each level the fraction amount κ of the corresponding cartilage tissue (index c) and soft tissue (index s) and with $E_c = 400$ kPa, $E_s = 60$ kPa, $\rho_c = 1140$ kg/m^3, $\rho_s = 1060$ kg/m^3, we have that the effective wall tissue density is:

$$\rho_{\text{wall}} = \kappa\rho_c + (1-\kappa)\rho_s. \tag{2.13}$$

In the previous elastic case [17], Hooke's law was employed, i.e. the stress is related to the strain by the linear relation:

$$\sigma = E\epsilon \tag{2.14}$$

with the effective elastic modulus calculated as: $E = \kappa E_c + (1-\kappa)E_s$ for each airway generation. However, this is not valid in case of viscoelastic airway walls, as shown in [35]. In the present study, the strain measure is given by $\epsilon = \zeta/R$ and the uniaxial stress σ has been substituted by its fraction $\sigma_D = \sigma/(1-\nu_P^2)$. The equivalent of (2.14) is the ratio between stress and strain of the lung parenchymal tissue with the Young's moduli E.

To incorporate the new constitutive equation in the present model of human lungs, let us come back to our previous model and calculation from [17]. In our sequel, the modelling of the motion of the relatively short airway ducts has been limited to radial movement of the tube. Hence its motion has been described by the function $\zeta(z,t)$ of the axial variable z and the time t. For the strain measure ϵ, the ratio ζ/R where R is the initial radius of the tube, has been adopted and the corresponding strain rate measure will be given by:

$$\frac{\partial\epsilon}{\partial t} = \frac{1}{R}\frac{\partial\zeta}{\partial t}. \tag{2.15}$$

In the case of viscoelastic model of the airway wall, the Voigt body model [6, 8] can be asumed. The Voigt body is the simplest viscoelastic model that can store and dissipate energy. It consists of a perfectly elastic element, i.e. a spring, arranged in parallel with a purely viscoelastic element, i.e. a dashpot. Its constitutive equation for the stress σ in terms of the strain ϵ is:

$$\sigma = E\epsilon + \eta\frac{\partial\epsilon}{\partial t}, \tag{2.16}$$

where E represents the elastic constant of the string and η is the viscous coefficient of the dashpot. This observation together with (2.16)–(2.15), leads to the following expression for the uniaxial stress in the wall of the tube:

$$\sigma_D = \frac{E}{1-\nu_P^2}\frac{\zeta}{R} + \frac{\eta}{R(1-\nu_P^2)}\frac{\partial\zeta}{\partial t}. \tag{2.17}$$

2.3. A fractional order lumped model of viscoelasticity

The viscoelasticity of the wall determined by the rheological properties of the tissue and described by (2.16) does not take into account the stress relaxation

effect, because in the process under constant strain $\epsilon(t) = \epsilon(t_0)$ for $t > t_0$, the stress does not change, since then the strain rate is zero and consequently $\sigma(t) = E\epsilon(t) = E\epsilon(t_0)$. Taking the time derivative of (2.16), we get:

$$\frac{\partial\sigma(t)}{\partial t} = E\frac{\partial\epsilon}{\partial t} + \eta\frac{\partial^2\epsilon(t)}{\partial t^2}. \tag{2.18}$$

This equation does not show relaxation either. Let us add to the right-hand side of the last equation an extra term proportional to the strain, i.e. $H\epsilon$, with the new material parameter H. We obtain a new constitutive law:

$$\frac{\partial\sigma(t)}{\partial t} = E\frac{\partial\epsilon}{\partial t} + \eta\frac{\partial^2\epsilon(t)}{\partial t^2} + H\epsilon(t). \tag{2.19}$$

Notice that this constitutive equation takes into account relaxation, because in the process under constant strain $\epsilon(t) = \epsilon(t_0)$ for $t > t_0$, the stress will change. Since the strain rate is zero, the extra term will give the stress rate:

$$\frac{\partial\sigma(t)}{\partial t} = H\epsilon(t_0), \tag{2.20}$$

and consequently $\sigma(t) = \sigma(t_0) + (t - t_0)H\epsilon(t_0)$. Notice that in the relaxation process we are expecting a decay of the stress to zero, which takes place only if H is negative. Relation (2.19) is a mixture of the Maxwell and Voigt models of linear viscoelasticity.

Finally, both the Maxwell-element, as well as the Kelvin–Voigt-element, do not fully characterize the true viscoelastic behaviour. Hence, combining of both elements seems to be a good solution to overcome their individual limitation: N parallel Maxwell-elements, all in parallel with an extra spring, as shown in Fig. 1.

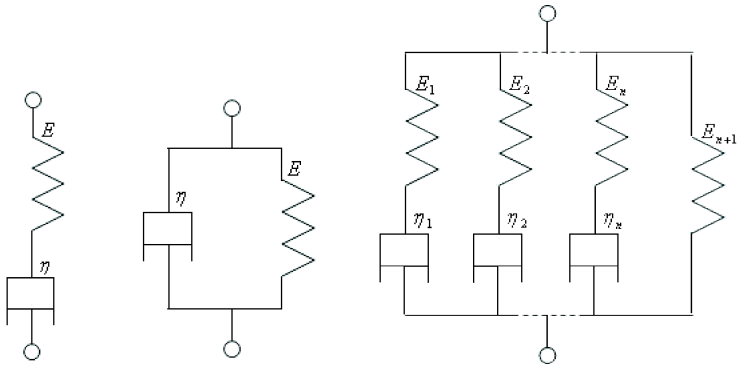

FIG. 1. From left to right: the Maxwell- and the Kelvin–Voigt-element, followed by a combination of the two.

For linear 1D viscoelastic material of Voigt type the classical Young modulus, denoted by E, after the Fourier transform of (2.16) does not get any frequency term as a product, due to the relation

$$E_V^*(i\omega) = \frac{\hat{\sigma}(\omega)}{\hat{\epsilon}(\omega)} = E + \eta i\omega. \tag{2.21}$$

If we apply the Fourier transform to the the second law of the mixture type (2.19), we get

$$E_M^*(i\omega) = \frac{\hat{\sigma}(\omega)}{\hat{\epsilon}(\omega)} = E + i(\eta\omega - H/\omega)\ , \tag{2.22}$$

which means a nonlinear dependence of complex viscoelastic modulus E_M^* on frequency. The question arises whether this nonlinear relation is in accordance with clinic observations or how to model different type relations. To answer this question, we refer to the concept of fractional order calculus (FOC) integral in characterizing the viscoelastic properties of the arterial walls modeled by Craiem and Armentano [8]. Clinic observations have shown that complex interactions in the lung tissue are significant at low frequencies [4], i.e. close to the breathing frequency, making unbiased identification a very difficult task. Moreover, elastin plays an important role in determining the rheological behavior of soft tissue, which in turn leads to the appearance of FOC differ-integration [36, 37]. The viscoelastic properties of lung tissue cause the effective tissue resistance to be very high at very low frequencies, but then to decrease asymptotically towards zero, at higher frequencies. Consequently, the tissue resistance has the main contribution to the total lung resistance. At breathing frequencies in the range of 0.2–0.4 Hz, tissue resistance can account for $\approx 40\%$ of the lung resistance.

Our previous observations show that in case of a whole model of the respiratory system with input impedance, both the integral and differential FOC must be present. Due to the complex nonlinear phenomena exhibited in the lung parenchyma and its intrinsic viscoelastic nature, it is difficult to relate the mechanical properties of the lungs to integer order differential system, like the mixed Maxwell–Voigt model (2.19). It is clear that fractional calculus offers handy tools to characterize such complex dynamics. It is also challenging to explain viscoelasticity in relation to lung pathology.

Fractional order calculus stems from the beginning of the theory of differential and integral calculus [24, 25, 30] and has been a fruitful field of research in science and engineering. In seems that in the last two decades, fractional differentiation has played an increasing role in various fields such as mechanics (viscoelasticity/damping,), electricity, electronics, chemistry, biology, economics and notably control theory, robotics, image and signal processing, diffusion and wave propagation [10, 33, 38].

Another and very broad field of recent applications of FOC is biomechanics. Some diseases (such as osteoporosis) are caused by biochemical and hormonal changes in human body. They lead to modification of the structure and composition of bones such as porosity and thickness of trabeculae, as well as to mineral density changes. Since trabecular bone is an inhomogeneous porous medium with viscoelastic properties, to measure those changes ultrasonic methods are used. The interaction between the ultrasound and the bone is highly complex. Modelling of ultrasonic propagation through trabecular tissue has been considered by using porous media theories, e.g. Biot's theory. Many authors have used fractional calculus as an empirical method to describe the properties of porous and viscoelastic materials [10, 33]. We are following this line-of-thought in modelling of the lung tissue.

There are two different viewpoints to the fractional calculus: the continuous-time viewpoint based on the Riemann–Liouville fractional integral [25] and the discrete-time viewpoint based on the Grünwald–Letnikov fractional derivative [30]. Both approaches turn out to be useful in treating situations of practical application in different fields, including numerical analysis, physics, engineering, biology, economics and finance.

Take any real-valued function $h(t)$ defined on $\mathbf{R}^+ = [0, \infty)$; by a *fractional derivative of order* $\alpha \in \mathbf{R}$ of h we understand a function defined on $[0, \infty) =: \mathbf{R}^+$ with its value in $\mathbf{R}$, given by the classical Caputo definition [30] as

$$\frac{d^\alpha h(t)}{dt^\alpha} = \frac{1}{\Gamma(n-\alpha)} \int_0^t \frac{h^{(n)}(\tau)}{(t-\tau)^{\alpha+1-n}} d\tau, \tag{2.23}$$

for $n - 1 < \alpha \leq n$. If $\alpha = n$ then

$$\frac{d^\alpha h(t)}{dt^\alpha} = h^{(n)}(t); \tag{2.24}$$

here $h^{(n)}(\tau)$ denotes the nth-order derivative of the function $h(\tau)$, $\tau \in \mathbf{R}^+$ and Γ is the Euler gamma function, which generalizes the factorial to non-integer values[1)], i.e. $\Gamma(x+1) = x\Gamma(x)$ when $x > 0$.

Integer order derivatives are local operators, fractional, i.e. real order derivatives, on the other hand, are non-local ones. Following (2.23) they can be seen as the convolution of $h(t)$ with a $t^{n-1-\alpha}$ function, anticipating some memory capability and power-law responses. In FOC negative order derivatives correspond to integration, and the following formula holds which is an equivalence of the

[1)]The function is extended to negative values by the definition $\Gamma(x) = \Gamma(x+1)/x$, then $\Gamma(-1/2) = -2\Gamma(1/2)$. An extension to complex argument also exists.

Fourier transformation of integer order derivatives

$$\widehat{\frac{d^\alpha h(t)}{dt^\alpha}} = (i\omega)^\alpha \hat{h}(\omega). \tag{2.25}$$

If we pass, like Craiem and Armentano [8], to the fractional order derivatives in the last Equation (2.19), with different orders α and β for strain and stress, respectively, then we get

$$\frac{\partial^\beta \sigma(t)}{\partial t^\beta} = E\frac{\partial^\beta \epsilon}{\partial t^\beta} + \eta\frac{\partial^{\alpha+\beta}\epsilon(t)}{\partial t^{\alpha+\beta}} + H\epsilon(t), \tag{2.26}$$

where $0 \leq \alpha, \beta \leq 1$. If we take the integral of fractional order β of the both sides of (2.26), we obtain:

$$\sigma(t) = E\epsilon(t) + \eta\frac{\partial^\alpha \epsilon(t)}{\partial t^\alpha} + H\frac{\partial^{-\beta}\epsilon(t)}{\partial t^{-\beta}}. \tag{2.27}$$

Taking the Fourier transform of the last relation we get:

$$\hat{\sigma}(\omega) = (E + \eta(i\omega)^\alpha + H(i\omega)^{-\beta})\hat{\epsilon}(\omega). \tag{2.28}$$

Now we can pass to our model of respiratory system with periodic breathing condition (2.1), (2.8). Then it is helpful to introduce the complex value material (pseudoelastic) modulus E^* which is a composition of both the material coefficients E and η and the function of frequency ω appearing on the RHD of (2.28) in front of $\hat{\epsilon}$, namely:

$$E^* = E_{\mathrm{re}} + iE_{\mathrm{im}}, \tag{2.29}$$

where

$$E_{\mathrm{re}} = E + \eta\cos\left(\frac{\pi\alpha}{2}\right)\omega^\alpha + H\cos\left(\frac{-\pi\beta}{2}\right)\omega^{-\beta},$$

$$E_{\mathrm{im}} = \eta\sin\left(\frac{\pi\alpha}{2}\right)\omega^\alpha + H\sin\left(\frac{-\pi\beta}{2}\right)\omega^{-\beta}.$$

Its form will be used in the further calculation of the complex modulus of elasticity. Notice that the case of the classical Voigt material is included here, under the condition: $\alpha = 1$, $\beta = 0$.

2.4. Balance equation for viscoelastic thick-walled tube

To write the balance equation for an arbitrary element of the tube wall confined by the inner radius R and the outer radius $R + h$, the radial angles θ_1, θ_2 and the boundaries in the axial directions z_1, z_2, we assume, that on the tube at the inner radius R only the air pressure P acts, while the outer radius is

stress-free [17]. Hence the equation of motion of the infinitesimal element $d\theta dz$, where $d\theta = \theta_2 - \theta_1$ and $dz = z_2 - z_1$ with thickness h follows, as in [17], from the second law of motion which states the balance of gravitational, inner and inertial forces. The gravitational forces are neglected and the inner forces are the pressure p and the stress σ_D. Knowing that the inertial force is the effective mass density ρ_{wall} times the volume and the acceleration, it follows that:

$$p(R+\zeta)d\theta dz + h\sigma_D d\theta dz = h\rho_{\text{wall}}(R+\zeta)d\theta dz\frac{\partial^2\zeta}{\partial t^2}, \tag{2.30}$$

where σ_D is given by (2.17). Notice that (2.30) is valid for any increment $d\theta dz$. Assuming a negligible displacement ζ in comparison to R, we may divide both sides of (2.30) by $Rd\theta dz$, to get:

$$p + h\frac{\sigma_D}{R} = h\rho_{\text{wall}}\frac{\partial^2\zeta}{\partial t^2}. \tag{2.31}$$

Now incorporating the constitutive equation (2.17) for the stress, we obtain that:

$$p + h\frac{1}{R}\left(\frac{E}{1-\nu_P^2}\frac{\zeta}{R} + \frac{\eta}{R(1-\nu_P^2)}\frac{\partial\zeta}{\partial t}\right) = h\rho_{\text{wall}}\frac{\partial^2\zeta}{\partial t^2}\,. \tag{2.32}$$

If we arrange the appropriate terms, then we have:

$$p + \frac{h}{R^2(1-\nu_P^2)}\left(E\zeta + \eta\frac{\partial\zeta}{\partial t}\right) = h\rho_{\text{wall}}\frac{\partial^2\zeta}{\partial t^2}\,. \tag{2.33}$$

Here we can use a more general constitutive law describing viscous effects given by fractional order derivative (2.26) or (2.27). Then we get

$$p + \frac{h}{R^2(1-\nu_P^2)}\left(E\zeta + \eta\frac{\partial^\alpha\zeta(t)}{\partial t^\alpha} + H\frac{\partial^{-\beta}\zeta(t)}{\partial t^{-\beta}}\right) = h\rho_{\text{wall}}\frac{\partial^2\zeta}{\partial t^2}\,. \tag{2.34}$$

From this one can obtain new relation for a given oscillatory frequency (or an interval of frequencies).

Let us now summarize the model developed hitherto. The model for wave propagation as a function of the pressure p (kPa), for axial w (m/s) and radial u (m/s) velocities, for flow q (l/s), and for the wall deformation ζ at the axial distance $z = 0$, is based on our previous studies and is given by the equations [17]:

$$p(t) = Ae^{i(\omega t - \phi_P)}, \tag{2.35}$$

$$u(y,t) = \frac{RA\omega}{2\rho\acute{c}_0^2}\cdot\frac{\acute{M}_{10}(y)}{\acute{M}_{10}}\cos\left(\omega t - \acute{\varepsilon}_{10} - \phi_P + \acute{\varepsilon}_{10}(y) + \frac{\pi}{2}\right), \tag{2.36}$$

$$w(y,t) = \frac{R^2A\omega}{\acute{c}_0\mu\sqrt{\acute{M}_{10}}}\cdot\frac{\acute{M}_0(y)}{\delta^2}\sin\left(\omega t - \frac{\acute{\varepsilon}_{10}}{2} - \phi_P + \acute{\varepsilon}_0(y) + \frac{\pi}{2}\right), \tag{2.37}$$

$$q(t) = \frac{\pi R^4}{\mu} \cdot \frac{A\omega}{\acute{c}_0 \sqrt{\acute{M}_{10}}} \cdot \frac{\acute{M}_{10}}{\delta^2} \sin\left(\omega t + \frac{\acute{\varepsilon}_{10}}{2} - \phi_P + \frac{\pi}{2}\right), \tag{2.38}$$

$$\zeta(t) = \frac{A}{\frac{hE^*}{R^2} - \rho_{\text{wall}} h\omega^2} \cos(\omega t - \phi_P), \tag{2.39}$$

with $A = 2R\left(\frac{E^*}{1-\nu^2}\frac{h}{R^2} - \rho_{\text{wall}} h\omega^2\right)$, and where:

$$\acute{c}_0 = \sqrt{E^* h/(2\rho R(1-\nu^2))}. \tag{2.40}$$

We denote by $\acute{M}_0, \acute{M}_{10}, \acute{\acute{M}}_{10}$ the moduli, and by $\acute{\varepsilon}_0, \acute{\varepsilon}_{10}, \acute{\acute{\varepsilon}}_{10}$ the phase angles of Bessel functions of the first kind and order 0, respectively 1 [1], as in:

$$\begin{aligned} \acute{M}_0(y) e^{i\acute{\varepsilon}_0(y)} &= 1 - J_0(\delta i^{3/2} y)/J_0(\delta i^{3/2}), \\ \acute{M}_{10} e^{i\acute{\varepsilon}_{10}} &= 1 - 2J_1(\delta i^{3/2})/(J_0(\delta i^{3/2})\delta i^{3/2}), \\ \acute{\acute{M}}_{10}(y) e^{i\acute{\acute{\varepsilon}}_0(y)} &= 1 - 2J_1(\delta i^{3/2} y)/(J_0(\delta i^{3/2})\delta i^{3/2}). \end{aligned} \tag{2.41}$$

Equations (2.35)–(2.39) represent the model developed in [17]. This model is derived from the previous works of [26, 27, 29, 34], which are based on the classical fluid dynamics theory and hydraulics [41]. The derivation of the model is presented in detail in [34], applied to the cardiovascular system. In our sequel [17] we have adapted this model to the conditions of the respiratory tree.

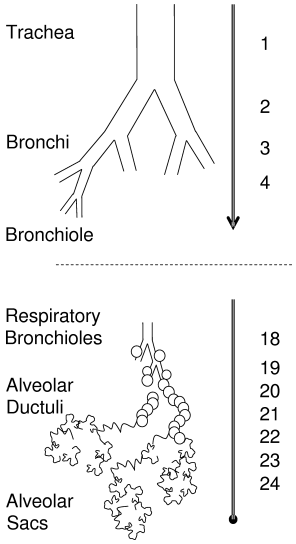

Fig. 2. Schematic representation of the bronchial tree: generations 1–16 transport gas and 17–24 provide gas exchange [40].

We introduced viscoelasticity in (2.29), assuming that the viscoelastic behaviour of the airway walls was a complex function, yielding a real and an imaginary part [6, 8, 35]. Relation (2.29) can be then written as a corresponding modulus and phase: $E^* = E_{\mathrm{re}} + iE_{\mathrm{im}} = |E|e^{i\varphi_E}$. The complex definition of elasticity will change the form of the wave velocity from (2.40) to:

$$\acute{c}_0 = \sqrt{\frac{|E|he^{i\varphi_E}}{2\rho R(1-\nu^2)}} = \sqrt{\frac{|E|h}{2\rho R(1-\nu^2)}}e^{0.5i\varphi_E}. \tag{2.42}$$

2.5. Electrical modelling of pressure-flow dynamics

By analogy to electrical networks [7], one can consider voltage P to be equivalent for respiratory pressure p and current Q as equivalent for air-flow q (see Table 2). Electrical resistances R_e represent respiratory resistance that occurs as a result of airflow dissipation in the airways, electrical capacitors C_e represent volume compliance of the airways which allows them to inflate/deflate, and electrical inductors L_e represent inertia of the air [17]. Additionally to these components, we introduce the viscous losses represented by equivalent electrical conductance G_e. These properties are often clinically referred to as mechanical properties: resistance, compliance, inertance and conductance; and this section will describe them in function of airway morphology.

Table 2. The electromechanical analogy.

Electrical	Mechanical
Voltage [V]	Force [N]
Current [A]	Velocity [m/s]
Resistance R_e [Ω]	Damping constant B [N · s/m]
Capacitance C_e [F]	Spring constant $1/K$ [m/N]
Inductance L_e [H]	Mass M [kg]

Consider a transmission line cell as a 2-input/output system depicted in Fig. 3. Using the relations $\sinh(\gamma x) = (e^{\gamma x} - e^{-\gamma x})/2$, $\cosh(\gamma x) = (e^{\gamma x} + e^{-\gamma x})/2$, we can write the relationship between the input $x = -\ell$ and the output $x = 0$ as:

$$\begin{bmatrix} P_1 \\ Q_1 \end{bmatrix} = \begin{bmatrix} \cosh(\gamma\ell) & Z_0 \sinh(\gamma\ell) \\ \dfrac{1}{Z_0}\sinh(\gamma\ell) & \cosh(\gamma\ell) \end{bmatrix} \begin{bmatrix} P_2 \\ Q_2 \end{bmatrix}, \tag{2.43}$$

with $\gamma = \sqrt{(r_x + i\omega l_x)(g_x + i\omega c_x)} = \sqrt{Z_l/Z_t}$ being the propagation constant, $Z_0 = \sqrt{(r_x + i\omega l_x)/(g_x + j\omega c_x)} = \sqrt{Z_l Z_t}$ – the characteristic impedance and $Z_l = r_x + i\omega l_x = \gamma Z_0$ – the longitudinal impedance, respectively

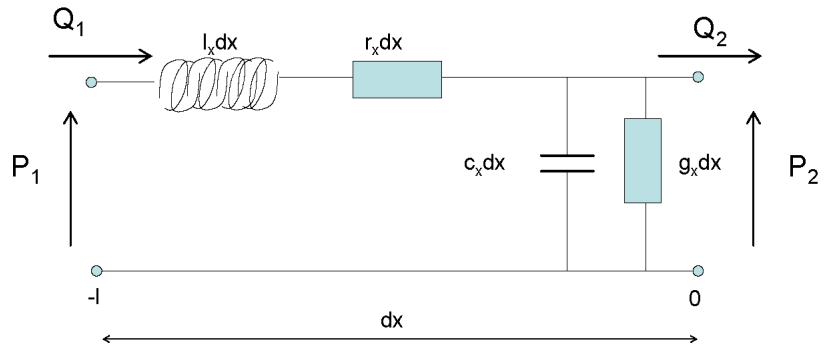

Fig. 3. Schematic representation of the infinitesimal distance dx over the transmission line and its parameters.

$Z_t = 1/(g_x + j\omega c_x) = Z_0/\gamma$ – the transversal impedance. The relation for the longitudinal impedance in function of aerodynamic variables is given by

$$Z_l = \frac{i\omega\rho}{\pi R^2 \acute{M}_{10}} e^{-i\acute{\varepsilon}_{10}} = \frac{\mu\delta^2}{\pi R^4 \acute{M}_{10}} e^{-i(\frac{\pi}{2}-\acute{\varepsilon}_{10})} = \frac{\mu\delta^2}{\pi R^4 \acute{M}_{10}} [\sin(\acute{\varepsilon}_{10}) + i\cos(\acute{\varepsilon}_{10})],$$

respectively, in terms of transmission line parameters, the longitudinal impedance is given by $Z_l = r_x + i\omega l_x$. By equivalence of the two relations we have that the resistance per unit distance is:

$$r_x = \frac{\mu\delta^2}{\pi R^4 \acute{M}_10} \sin(\acute{\varepsilon}_{10}). \tag{2.44}$$

It follows that $\omega l_x = \dfrac{\mu\delta^2}{\pi R^4 \acute{M}_{10}} \cos(\acute{\varepsilon}_{10})$ and recalling that $\delta = R\sqrt{\dfrac{\omega\rho}{\mu}}$, the inductance per unit distance is:

$$l_x = \frac{\rho}{\pi R^2} \frac{\cos(\acute{\varepsilon}_{10})}{\acute{M}_{10}}. \tag{2.45}$$

In case of a viscoelastic pipeline, the characteristic impedance is given by

$$Z_0 = \frac{\rho}{\pi R^2} \frac{1}{1-\nu_P^2} \sqrt{\frac{|E|\,h}{2\rho R}} \frac{1}{\sqrt{\acute{M}_{10}}} e^{-i(\frac{\acute{\varepsilon}_{10}}{2}+\frac{\varphi_E}{2})}$$

and the transversal impedance is given by

$$Z_t = \frac{1}{g_x + i\omega c_x} = \frac{Z_0^2}{Z_l} = 1/\left(\omega \frac{2\pi R^3 (1-\nu_P^2)^2}{|E|\,h} e^{i(\frac{\pi}{2}-\varphi_E)}\right),$$

from where the conductance per unit distance can be extracted:

$$g_x = \omega \frac{2\pi R^3 (1-\nu_P^2)^2}{|E|\,h} \sin\varphi_E \tag{2.46}$$

and the capacitance per unit distance is given by:

$$c_x = \frac{2\pi R^3(1-\nu_P^2)^2}{|E|\,h}\cos\varphi_E. \tag{2.47}$$

Thus, from the geometrical (R, h) and mechanical (E^*, ν_P) characteristics of the airway tube, and from the air properties (μ, ρ), one can express the r_x, l_x, g_x and c_x parameters. In this way, the dynamic model can be expressed in an equivalent transmission line defined by Eqs. (2.44)–(2.47). Since $|\gamma| \ll 1$, we can estimate that over the length ℓ of an airway tube (thus $x = \ell$), we have the corresponding properties:

$$R_e = r_x\ell = \ell\frac{\mu\delta^2}{\pi R^4 \acute{M}_{10}}\sin(\acute{\varepsilon}_{10}), \tag{2.48}$$

$$L_e = l_x\ell = \ell\frac{\rho}{\pi R^2}\frac{\cos(\acute{\varepsilon}_{10})}{\acute{M}_{10}}, \tag{2.49}$$

$$G_e = g_x\ell = \ell\omega\frac{2\pi R^3(1-\nu_P^2)^2}{|E|\,h}\sin\varphi_E, \tag{2.50}$$

$$C_e = c_x\ell = \ell\frac{2\pi R^3(1-\nu_P^2)^2}{|E|\,h}\cos\varphi_E. \tag{2.51}$$

Some more details are given in the Appendix.

2.6. Applications

The set of equations given by (2.35)–(2.39) can be used to investigate the variations in tidal breathing pressure and flow waves caused by pathology in the nominal function of the lung. Tidal breathing means that air goes into the lungs the same way that it comes out; in other words, it characterizes the inhalation and exhalation at rest (no forceful maneuvers, no exercise, etc.). In this paper, we shall investigate only the normal (healthy) case. However, one may expect that variations in pressure and flow patterns from specific diseases will have effect on the mechanical parameters (2.48)–(2.51), changing the total values of the respiratory input impedance. Due to the fact that the network is dichotomous and symmetric, we can obtain the total mechanical impedance using the network structure as in Fig. 4, with B_m and K_m calculated with the electro-mechanical equivalence from Table 2. Since the Kelvin–Voigt elements corresponding to one level are in parallel, their transfer function H_m will be in series with the spring in the level $m-1$. The next corresponding transfer function is in parallel with the damper in the level $m-1$, as depicted schematically by Fig. 4. In this manner, the total transfer function $H(s)$ can be determined, starting at level 24.

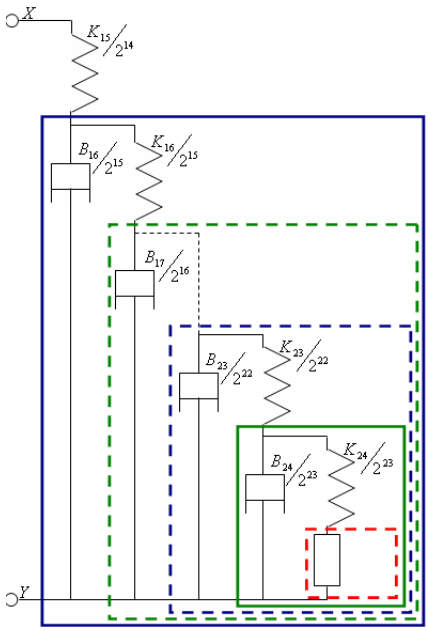

Fig. 4. A schematic representation of how the mechanical impedance $H(s)$ is calculated from level 24 (red dashed box) by adding consequent levels (green box, blue dashed box, etc.) up to level 16.

Hence, in this representation, the stress and strain properties can be evaluated using (2.16). The strain is increased in steps of 10%, from 10% to 100%. Starting from level 24, one can then calculate the stress-strain curve at the input of each level. This then will give rheological information in the context that all parenchymal levels are interconnected, hence in a combination of Maxwell–Kelvin–Voigt elements. Notice that here we show the stress-strain only for the respiratory parenchyma (levels 16–24).

2.7. Measurements in the 4–48 Hz frequency range

In order to compare the results obtained by the nominal simulator parameters with measured data from healthy patients, an averaged impedance has been made from 25 healthy subject whose biometric characteristics are given in Table 3 [18]. These subjects have been tested for their lung function using the forced

Table 3. Biometric parameters of the healthy subjects. Values are presented as mean ± SD, as from [18].

	Healthy
Age (yrs)	26 ± 3
Height (m)	1.67 ± 0.04
Weight (kg)	64 ± 3.7

oscillation technique [28]. From the non-invasive measurement of the air-pressure and air-flow at the mouth, the complex impedance is obtained, and its equivalent Bode and polar characteristics [15]. The range of frequencies where the data is measured varies between 25 rad/s and 300 rad/s (i.e. from 4 to 48 Hz).

2.8. Measurements in the 0.1–5 Hz frequency range

Since viscous effects are visible at low frequencies, we need to validate our model at low frequencies (i.e. below 5 Hz). For the purpose of this validation, we use the data reported in the specialized literature. The first set consists of impedance data in healthy subjects in the frequency range between 0.25 and 5.0 Hz [14]. The measurements were taken in normal breathing conditions, using the forced oscillation technique. The second set of impedance data consists of ventilated anesthetized patients during cardiac surgery between 0.2 and 2.0 Hz [3]. The two data sets were selected from the published papers and approximated using the corresponding figures.

3. Results

The variations with each generation for the mechanical parameters resistance, iterance, capacitance and conductance are given in Fig. 5. This variation becomes linear when plotted as a logarithmic function, whereas it becomes exponential when plotted linearly.

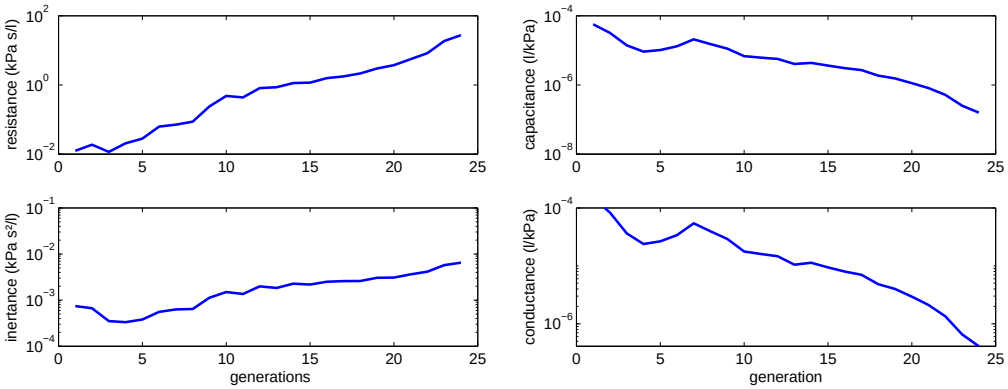

FIG. 5. Variations in: resistance, iterance, capacitance and conductance for nominal (continuous line), case.

Figure 6(left) depicts the evolution of the mechanical parameters in a single tube at a certain level m, whereas Fig. 6(right) depicts their evolution in the entire level. One may observe that the evolution in a single tube, in consecutive levels is quasi-linear for both parameters (Fig. 6(left)). However, since the

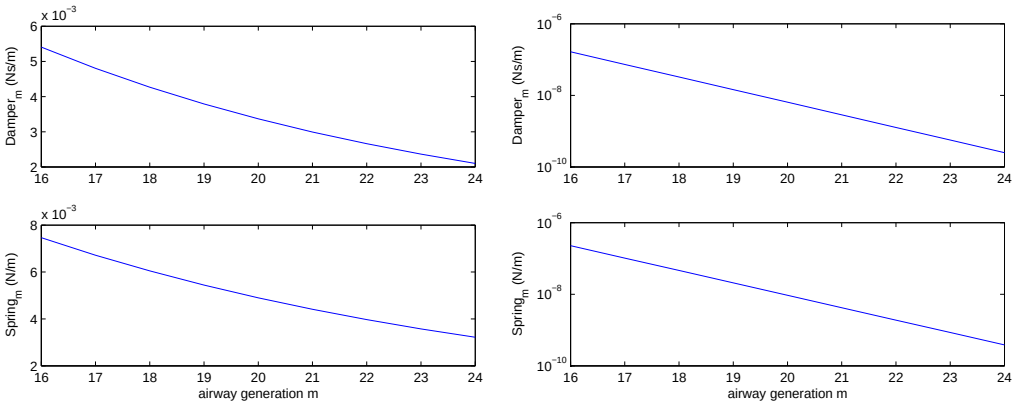

Fig. 6. Parameter evolution in singular tubes (left) and in the entire level (right), for levels 16–24.

total parameter values from Fig. 6(right) depend on the total number of tubes within each level, they change as an exponential decaying function. When represented in a logarithmic scale, one can observe a quasi-linear behavior, as in Fig. 6(right).

The stress-strain curves are depicted in Fig. 7. As expected, the stress increases with the degree of elongation applied to the entire structure. The more levels we have in our structure, the higher will be the values of the stress-strain curve, due to higher amount of cartilage tissue (collagen).

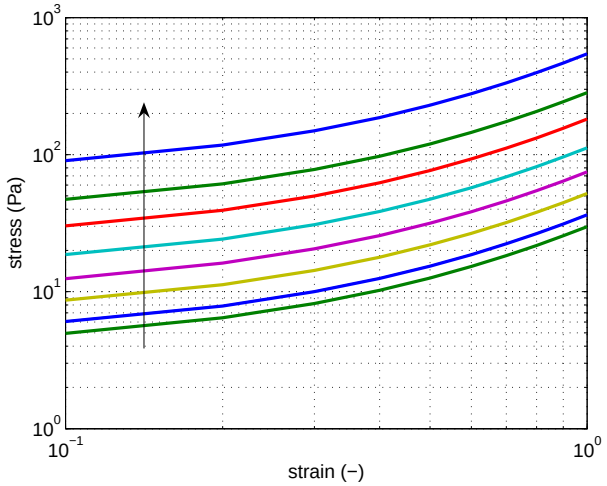

Fig. 7. The stress-strain curves. The vertical arrow denotes the evolution in each level, from a ladder network model of the cell 24, to ladder network models with additional cells, until all levels until 16 are included.

One can observe the fitting of the model to the averaged measured impedance in the 4–48 Hz frequency interval depicted in Fig. 8(left). Its equivalent polar plot is given in Fig. 8(right).

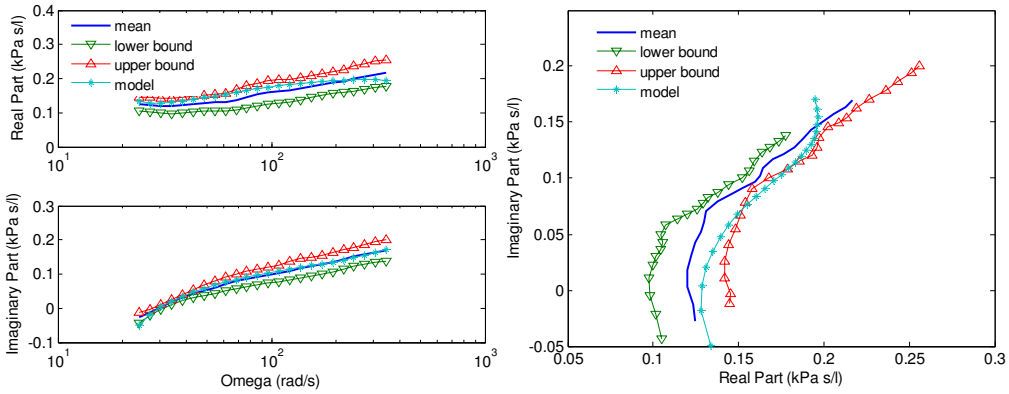

FIG. 8. Measured impedance in healthy subjects as averaged values with upper and lower bounds (left); model fitting (right).

The evolution with frequency of the mechanical impedance as per level or as a total branching network is given in Fig. 9. One may observe that at low frequencies the frequency dependence becomes significant.

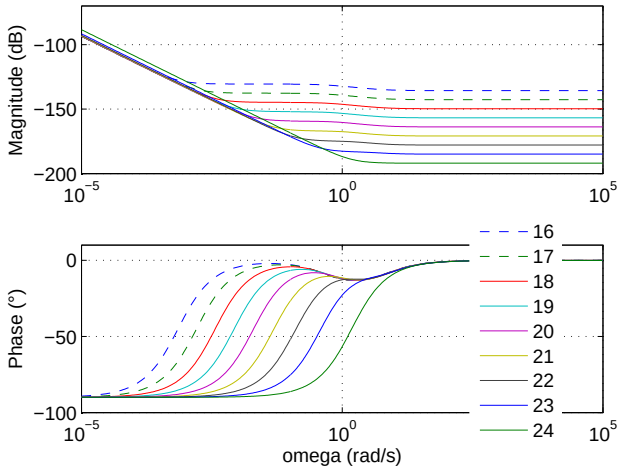

FIG. 9. Variations in the mechanical impedance with each airway generation level.

Evaluation of the lumped model $Z_{id} = R_{id} + 1/(C_{id}s^{\beta})$ in the lower frequency range is done on the data known from literature, Z_r. Figure 10 depicts the

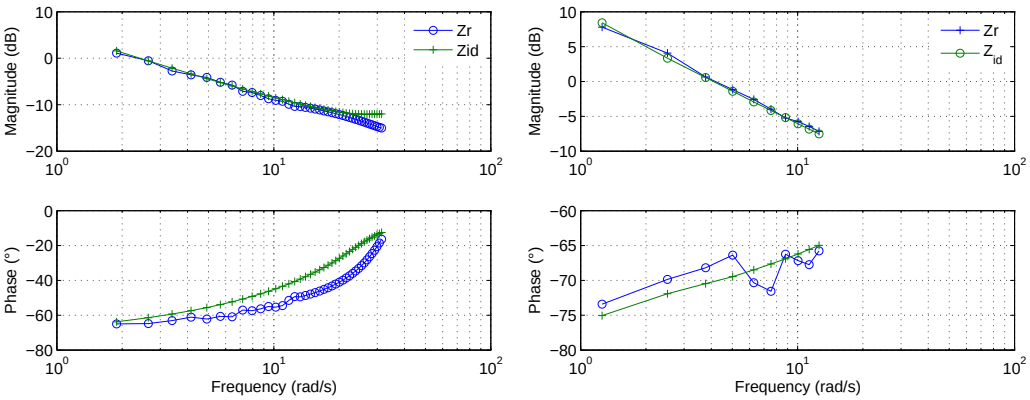

Fig. 10. Impedance data Z_r from literature [14] (left) and from [3] (right), and the fitted lumped model Z_{id}.

fitting of the model on the two data sets from literature. The model values for Fig. 10(left) are: total resistance 0.1332 (kPa s/l), compliance 0.5274 (l/kPa) and a fractional order of β=0.8095. The model values for Fig. 10(right) are: total resistance 0.0488 (kPa s/l), compliance 0.3274 (l/kPa) and a fractional order of β=0.8035.

4. Discussion

The results presented here are in agreement with previous studies and show that predominant pressure drop occurs in the upper airways (first 5 bifurcation levels) [26]. The results depend strongly on the airway wall viscoelasticity, which is varying in disease. For typical flow rates during spontaneous breathing ranging 0.5–1 l/s, wall roughness is neglected since it has little effect in laminar flow conditions and for low values of the Womersley parameter [19]. In the respiratory system, the values of δ are always less than 1, varying from 0.0471 in alveoli to 0.785 in the trachea. For the circulatory system, these values become as high as 24, causing deviations from the Poiseuille parabolic flow profile. Therefore, we can conclude that in our case the parabolic flow profile remains constant.

Our results are obtained under the following assumptions:

- laminar flow for typical Reynolds number during quiet breathing is less than 2000;
- ducts are long enough (this assumption is not true, thus neglecting the initial-flow length effects);
- the air is homogeneous and Newtonian;
- the axial velocity component is zero at the airway wall;
- uniform cylindrical duct (valid as approximation);

- for linearization we have assumed the following simplifications:
  a) $-\frac{\omega R}{c} \ll \delta$, which is true, for in respiration we have values between $3.5904e^{-5}$ and $2.1542e^{-6}$;
  b) the air velocity is small compared to the wave velocity; this is valid for most of the airways; i.e. in trachea there may be velocities as high as 10m/s, with a wave velocity of 339m/s;
  c) the values for y vary between $0 \to \pm 1$ (rigid pipe), although in reality it varies between $0 \to \pm(1 + \zeta/R)$ (viscoelastic pipe);
  d) the E^* modulus is dependent on the airway wall structure (cartilage fraction);
- thin-walled ducts; for the healthy respiratory system, the ratio h/R varies between 0.4625 in trachea, to 0.0896 in alveoli.

Due to the fact that we do not seek to obtain a precise/exact value of the components but merely a qualitative value, we assume that a more complex formulation may be correct and more realistic, but may improve little the overall conclusions.

For frequencies below 100Hz the transmission line theory can be applied in a simplified form, leading to the exact solution for pressure and flow changes in normal breathing conditions. A similar study has been employed in [27], leading to the same formula for the compliance (2.47). Similarity exists between the derivation of the input impedance in the respiratory tree in this study and modeling of the smaller systemic arteries, since in both simulations the symmetric structure is employed, along with laminar flow conditions, incompressibility, Newtonian fluid and the non-slip boundary conditions. The input impedance is extended to a more general tree in [27], by adding the equation of crossing a bifurcation based on a law on which the geometry changes over the junction. Nevertheless, we may argue that our choice of choosing to model a completely symmetric tree still reflects its essential behaviour.

Notice that in both impedance data, the models identified lower values in magnitude (or equivalently in the real part of complex impedance) in anesthetized subjects, is done by skipping the upper airways and measuring directly in the trachea (intubated patients). Since sedation provokes a relaxation of the parenchyma from a viscoelastic point of view, the compliance is lower in anesthetized patients than in those subjects during tidal breathing. This means that the lungs of the anesthetized patients are posing more resistance to changes in pressure, resulting in lower flow values. Typically, most of these patients are under artificial ventilation during surgery. The value of this fractional order in both modelling approaches is constant between the two sets of data. Since this order encompasses both the viscous and elastic elements, the fact that both sets of data come from subjects with healthy lung parenchyma, the identified values are similar.

It is straightforward to apply airway remodeling effects in this simple model representation, but limitations should be taken into account. The major errors which may occur in this study are determined by the heterogeneity of the human lung, i.e. inter-subject variability can affect the values from Table 1. However, these values are reported in several studies [12, 13, 20, 23, 40] and they had offered a good basis for investigations, originally measured from excised lungs [26, 39] and then in plastic casts [31, 32]. One should recall that this study aims to investigate the fractal-like geometry of the human lung, thus approximating it to a dichotomous tree is necessary. Even though the airway-tree of the human lung shows considerable irregularity, the principle of a systematic reduction of airway size seems to apply [21]. It was later demonstrated by a systematic analysis that the airway tree in different species shows a common fractal structure, in spite of some gross differences in airway morphology [42]. On the other hand, it is indeed interesting to quantify changes in the results if the degree of asymmetry (which is not much discussed in literature) in the respiratory tree is taken into account.

In terms of viscoelasticity, the elastic recoil of the lung is dominated at normal breathing frequencies (around 0.25 Hz) by the nonlinear stress-strain characteristics of the healthy lung tissue [6, 35]. It is agreed that the main stress-bearing constituents of lung tissue are collagen and elastin fibers. We have therefore achieved the respective changes in the airway wall structure, by affecting the balance between these two components.

5. Conclusions

In this paper, a mathematical model for the pressure and flow variations in the respiratory tree has been developed based on similarity to the well-defined Womersley theory, for oscillatory pressure and flow variations. The mathematical model is developed for tidal breathing conditions, which reflect the breathing at rest, allowing consequent assumptions to simplify the aero-dynamics (e.g. laminar flow conditions). The influence of changes in radius and elastic modulus with disease has been assessed in terms of mechanical parameters and total impedance. In simulations for viscoelastic airways, we have found that variations in these parameters correspond to the physiological insight and resemble the measured data.

The parameters developed here can be further used to investigate cases of pathologic subjects. The final aim is to obtain a direct relationship between variations in model parameters and lung pathology, which would be of great interest for clinical practice in follow-up studies and diagnosis. Additionally, these changes can be correlated to variations in values of fractional order model parameter, providing insight into the physiologic interpretation of such models.

A first step in this direction would be to replace the classical Voigt model for viscoelasticity by a non-integer order derivative model shortly presented here, as well.

Appendix A. Transmission line equivalence

We consider the analogy to voltage as being the pressure $p(x,t)$, and to current as being the air-flow $q(x,t)$, and we apply the transmission line theory. Here x denotes the current position of the line. We shall make use of the complex notation:

$$p(x,t) = P(x)e^{i(\omega t-\phi_P)}, \qquad q(x,t) = Q(x)e^{i(\omega t-\phi_Q)} \tag{A.1}$$

where x is the longitudinal coordinate (m), t is the time (s), ω is the angular frequency (rad/s), f is the frequency (Hz) and i is the complex unit $i=\sqrt{-1}$. The pressure and the flow are harmonics, with the modulus dependent solely on the location within the transmission line (dx). The transmission line equations link partial derivatives of p and g as follows:

$$\frac{\partial p(x,t)}{\partial x} = -r_x q - l_x \frac{\partial q}{\partial t}, \qquad \frac{\partial q(x,t)}{\partial t} = -g_x p - c_x \frac{\partial p}{\partial t}. \tag{A.2}$$

Introducing (A.1) in the first and second derivatives, gives, respectively:

$$\begin{aligned}
\frac{\partial P}{\partial x} &= -(r_x + i\omega l_x)Q = -Z_l Q,\\
\frac{\partial Q}{\partial x} &= -(g_x + i\omega c_x)P = -P/Z_t,\\
\frac{\partial^2 P}{\partial x^2} &= -(r_x + i\omega l_x)\frac{\partial Q}{\partial x} = -Z_l \frac{\partial Q}{\partial x},\\
\frac{\partial^2 Q}{\partial x^2} &= -(g_x + i\omega c_x)\frac{\partial P}{\partial x} = -\frac{\partial P}{\partial x}/Z_t,
\end{aligned} \tag{A.3}$$

with $Z_l = r_x + i\omega l_x$ the longitudinal impedance, and $Z_t = 1/(g_x + i\omega c_x)$ the transversal impedance. From (A.3) we obtain the system equations for $P(x)$ and $Q(x)$:

$$\frac{\partial^2 P}{\partial x^2} - Z_l P/Z_t = 0, \qquad \frac{\partial^2 Q}{\partial x^2} - Z_l Q/Z_t = 0. \tag{A.4}$$

Introducing the notation $\gamma = \sqrt{(r_x + i\omega l_x)(g_x + j\omega c_x)} = \sqrt{Z_l/Z_t}$, it follows that (A.4) can be rewritten as $\partial^2 P/\partial x^2 - \gamma^2 P = 0$ and $\partial^2 Q/\partial x^2 - \gamma^2 Q = 0$, to which the solution is given by $P(x) = Ae^{-\gamma x} + Be^{-\gamma x}$ and $Q(x) = Ce^{-\gamma x} + De^{-\gamma x}$ with complex coefficients A, B, C, D. Introducing this relation in (A.3), the system can be reduced to $Q(x) = 1/Z_0(Ae^{-\gamma x} - Be^{+\gamma x})$, with $Z_0 = \sqrt{(r_x + i\omega l_x)/(g_x + i\omega c_x)} = \sqrt{Z_l Z_t}$, in which Z_0 is the characteristic impedance of the transmission line cell.

Acknowledgement

Clara Ionescu acknowledges the financial support of the UGent-BOF grants nr. 011/V0103 and 011/D04506.

References

1. M. Abramowitz, I.A Stegun, *Handbook of Mathematical Functions with Formulas, Graphs, and Mathematical Tables*, Dover Publications, ISBN 978-0-486-61272-0, New York 1972.
2. A.P. Avolio, *A multibranched model of the human arterial system*, Med. and Biol. Eng. and Compl., **18**, 709–718, 1980.
3. B. Babik, T. Asztalos, F. Petak, Z. Deac, Z. Hantos, *Changes in respiratory mechanics during cardiac surgery*, Anesth. Analg., **96**, 1280–1287, 2003.
4. H. Bachofen, *Lung tissue resistance and pulmonary hysteresis*, J. Appl. Physiol., **24**, 296–301, 1968.
5. P.J. Barnes, *Chronic Obstructive Pulmonary Disease*, NEJM Medical Progress, **343**, 2, 269–280, 2000.
6. G. Maksym, J. Bates, *A distributed nonlinear model of lung tissue elasticity*, J. Appl. Physiol., **82**, 1, 32–41, 1997.
7. A.R. Bergen, V. Vittal, *Power system analysis*, 2nd ed., Pearson Education, United States of America, 1999.
8. D. Craiem, R. Armentano, *A fractional derivative model to describe arterial viscoelasticity*, Biorheology, **44**, 251–263, 2007.
9. H. Franken, J. Clément, M. Cauberghs, K. Van de Woestijne, *Oscillating flow of a viscous compressible fluid through a rigid tube: a theoretical model*, IEEE Trans. Biomed. Eng., **28**, 5, 416–420, 1981.
10. M. Fellah, Z.E.A. Fellah, C. Depollier, *Transient wave propagation in inhomogeneous porous materials: Application of fractional derivatives*, Signal Processing, **86**, 2658–2667, 2006.
11. A. Elizur, C. Cannon, T. Ferkol, *Airway inflammation in cystic fibrosis*, Chest, **133**, 2, 489–495, 2008.
12. S. Gheorghiu, S. Kjelstrup, P. Pfeifer, M.O. Coppens, *Is the lung an optimal gas exchanger?*, [in:] Fractals in Biology and Medicine, vol IV, G. Losa, D. Merlini, T. Nonnenmacher, E.R. Weibel [Eds.], Birkhaüser, Berlin, 31–42, 2005.
13. P. Harper, S. Karman, H. Pasterkamp, G. Wodicka, *An Acoustic Model of the Respiratory Tract*, IEEE Transactions of Biomedical Engineering, **48**, 5, 543–549, 2001.
14. Z. Hantos, B. Daroczy, B. Suki, G. Galgoczy, T. Csendes, *Forced oscillatory impedance of the respiratory system at low frequencies*, J. Appl Physiol., **60**, 1, 123–132, 1986.
15. C. Ionescu, R. De Keyser, *Parametric models for characterizing respiratory input impedance*, Taylor and Francis J. Med. Eng. and Tech., **32**, 4, 315–324, 2008.

16. C. IONESCU, R. DE KEYSER, *Relations between Fractional Order Model Parameters and Lung Pathology in Chronic Obstructive Pulmonary Disease*, IEEE Trans. Biomed. Eng., **56**, 4, 978–987, 2009.

17. C. IONESCU, P. SEGERS, R. DE KEYSER, *Mechanical properties of the respiratory system derived from morphologic insight*, IEEE Trans. Biomed. Eng., **56**, 4, 949–959, 2009; DOI: 10.1109/TBME.2008.2007807.

18. C. IONESCU, K. DESAGER, R. DE KEYSER, *Estimating respiratory mechanics with constant-phase models in healthy lungs from forced oscillations measurements*, Studia Universitatis "Vasile Goldis" Life Science Series, **19**, 1, 123–132, 2009.

19. M. KING, H.K. CHANG, M.E. WEBER, *Resistance of mucus-lined tubes to steady and oscillatory airflow*, J. Appl. Phys., **52**, 5, 1172–1176, 1982.

20. J.W. LEE, M.Y. KANG, H.J. YANG, E. LEE, *Fluid-dynamic optimality in the generation-averaged length-to-diameter ratio of the human bronchial tree*, Med. Bio. Eng. Comput., **45**, 1071–1078, 2007.

21. B. MANDELBROT, *The fractal geometry of nature*, Freeman and Co, NY 1983.

22. J. MEAD, *Mechanical Properties of Lungs*, Physiological Reviews, **41**, 2, 281–330, 1961.

23. B. MAUROY, *3D hydrodynamics in the upper human bronchial tree: interplay between geometry and flow distribution*, [in:] Fractals in Biology and Medicine, Vol. IV, G. LOSA, D. MERLINI, T. NONNENMACHER, E.R. WEIBEL [Eds.], Birkhaüser, Berlin, 43–53, 2005.

24. K. S. MILLER AND B. ROSS, *An Introduction to the Fractional Calculus and Fractional Differential Equations*, John Wiley and Sons, New York 1993.

25. K.B. OLDHAM, J. SPANIER, *The Fractional Calculus: Theory and Application of Differentiation and Integration to Arbitrary Order*, Academic Press, New York, London 1974.

26. D. OLSON, G. DART, G. FILLEY, *Pressure drop and fluid flow regime of air inspired into the human lung*, J. Appl. Physiol., **28**, 482–494, 1970.

27. M.S. OLUFSEN, *Structured tree outflow condition for blood flow in larger systemic arteries*, Heart Circ. Physiol., **45**, H257–H268, 1999.

28. E. OOSTVEEN, D. MACLEOD, H. LORINO, R. FARRE, Z. HANTOS, K. DESAGER, F. MARCHAL, *The forced oscillation technique in clinical practice: methodology, recommendations and future developments*, European Respiratory Journal, **22**, 1026–1041, 2003.

29. T. PEDLEY, R. SCHROTER, M. SUDLOW, *Flow and pressure drop in systems of repeatedly branching tubes*, J. Fluid Mech., **46**, 2, 365–383, 1971.

30. I. PODLUBNY, *Fractional Differential Equations*, Academic Press, San Diego 1999.

31. V. SAURET, K. GOATMAN, J. FLEMING, A. BAILEY, *Semi-automated tabulation of the 3D topology and morphology of branching networks using CT: application to the airway tree*, Phys. Med. Biol., **44**, 1625–1638, 1999.

32. V. SAURET, P. HALSON, I. BROWN, J. FLEMING, A. BAILEY, *Study of the three-dimensional geometry of the central conducting airways in man using computed tomographic (CT) images*, Journal of Anatomy, **200**, 123–134, 2002.

33. N. SEBAA, Z.E.A. FELLAHB,, W. LAURIKSA, C. DEPOLLIERC, *Application of fractional calculus to ultrasonic wave propagation in human cancellous bone*, Signal Processing, **86**, 2668–2677, 2006.

34. P. Segers, *Biomechanical modelling of the arterial system for non-invasive determination of arterial compliance*, PhD thesis [in Dutch], 1997, Ghent University, Chapters 1–3.

35. B. Suki, A.L. Barabasi, K. Lutchen, *Lung tissue viscoelasticity: a mathematical framework and its molecular basis*, J. Appl. Physiol., **76**, 6, 2749–2759, 1994.

36. B. Suki, H. Yuan, Q. Zhang, K. Lutchen, *Partitioning of lung tissue response and inhomogeneous airway constriction at the airway opening*, J. Appl. Physiol., **82**, 1349–1359, 1997.

37. B. Suki, *Biomechanics of the lung parenchyma: critical roles of collagen and mechanical forces*, J. Appl. Physiol., **98**, 1892–1899, 2005.

38. A.J. Turski, B. Atamaniuk, E. Turska, *Fractional derivative analysis of Helmholtz and paraxial-wave equations*, J. Tech. Phys., **44**, 2, 193–206, 2003.

39. E.R. Weibel, *Morphometry of the human lung*, Springer, Berlin 1963.

40. E.R. Weibel, *Mandelbrot's fractals and the geometry of life: a tribute to Benoît Mandelbrot on his 80th birthday*, [in:] Fractals in Biology and Medicine, vol. IV, G. Losa, D. Merlini, T. Nonnenmacher, E.R. Weibel [Eds.], Birkhaüser, Berlin, 3–16, 2005.

41. J. Welty, C. Wicks, R. Wilson, *Fundamentals of momentum, heat and mass transfer*, John Wiley and Sons, USA, 1969.

42. B.J. West, V. Barghava, A.L. Goldberger, *Beyond the principle of similitude: renormalization of the bronchial tree*, J. Appl. Physiol., **60**, 1089–1097, 1986.

43. J.R. Womersley, *An elastic tube theory of pulse transmission and oscillatory flow in mammalian arteries*, Wright Air Development Center, Technical Report WADC-TR56-614, 1957.

Received May 25, 2009; revised version December 17, 2009.